Pergamon

Int. J. Solids Structures Vol. 35, Nos 31-32, pp. 4275-4294, 1998

0020-7683/98 $19.00 + .00

PII: S0020-7683(97)00316-8

VERTICAL PENETRATION OF FLOATING ICE SHEETS

DEVINDER S. SODHI*

U.S. Army Cold Regions Research and Engineering Laboratory, 72 Lyme Road, Hanover, New Hampshire 03755-1290, U.S.A.

(*Received* 26 *July* 1996; *in revised form* 30 *May* 1997)

Abstract—Existing failure criteria for the bearing capacity of floating ice sheets predict the load for the occurrence of the first radial crack or a circumferential crack, when the maximum stress obtained from an elastic analysis in the ice equals the tensile strength. From full-scale and small-scale tests, the ultimate load to cause complete penetration of a floating ice sheet is much higher than that to cause the first radial crack. This can be attributed to wedging action during deformation of a radially cracked ice sheet. We present three approaches taken to determine the ice penetration force: (1) plastic limit analysis, (2) small-scale experiments, and (3) full-scale measurements in the field.

Small-scale experiments were conducted with freshwater ice in the basin at the laboratory to understand the wedging action during the vertical loading of floating ice sheets. Results of the following series of experiments are presented: (a) beams with fixed ends, (b) paired cantilever beams arranged free-end to free-end and loaded together, (c) beams with an apparatus inserted between the free ends of paired cantilever beams to measure the in-plane force during vertical loading, and (d) vertical downward loading of floating ice sheets with fixed and free boundaries. Analysis of the data from the beam tests reveals that the wedging action results in the development of wedging pressure in the top or bottom third of the ice thickness, and this results in a resisting moment that counters the deformation of a cracked ice sheet. An ice sheet attached to the basin wall inhibits the propagation of radial cracks because of the wedging action, whereas an ice sheet free at the edges from the surrounding ice sheet fails by the propagation of radial cracks all the way to the ice sheet's free boundary. The difference between the two breakthrough loads of the free and the fixed ice sheets can be attributed to wedging action. The results of the beam tests are used in the results of plastic limit analysis to predict the breakthrough loads of floating ice sheets, which are in agreement with loads measured during full-scale and small-scale experiments. © 1998 Elsevier Science Ltd. All rights reserved.

1. INTRODUCTION

In cold regions, floating ice sheets are often used as roads, airfields, parking lots, and construction platforms (Ashton, 1986). At times, submarines operating under the Arctic ice cover need to surface by lifting up and penetrating a floating ice sheet (Dane, 1993). To conduct these operations safely, it is important to know the breakthrough loads of floating ice sheets.

Because ice exists at temperatures close to its melting temperature, the creep of ice will lead to steadily increasing deflections under a static load. On the other hand, a floating ice sheet, when excited near its natural frequency of oscillations, will undergo deflections larger than those expected for static loads. Therefore, the response of a floating ice sheet depends on the duration and history of loading, which can fall into the following three categories (Ashton, 1986): (1) quasi-static loads, such as those imposed by slowly moving vehicles, (2) moving loads that may excite waves in the ice–water system to oscillate at or near its natural frequency, and (3) long-term loads, such as those imposed by parked vehicles, stored materials, or drilling platforms. In existing literature, ice is assumed to behave as an elastic material for evaluating the deflections of and stresses in an ice sheet due to short-term and moving loads, whereas creep deformation becomes important for long-term loads (Beltaos and Lipsett, 1979). Based on the results of laboratory and field tests, Sinha (1996) proposed that an elasto-delayed–elastic model for primary creep of ice can be combined with the result of elastic theory of plates on an elastic foundation (Hertz, 1884; Wyman 1950) to predict deflections due to short-term loads. In this paper, attention is focused on

* Tel.: 1-603-646-4267. Fax: 1-603-646-4477. E-mail: dsodhi@crrel.usace.army.mil.

short-term loading of floating ice sheets to failure. The load is applied over a given area and gradually increased until breakthrough takes place. The theoretical treatment of the bearing capacity of floating ice sheets is quite extensive and may be found in textbooks (e.g., Michel, 1978; Ashton, 1986) and in reports (e.g., Kerr, 1975; Nevel, 1976). However, the prediction of breakthrough loads for floating ice sheets is empirically based on full-scale experimental data.

Full-scale tests to determine breakthrough loads were conducted by Frankenstein (1963, 1966) on freshwater lake ice in Michigan, North Dakota, and Alaska, and by Lichtenberger *et al.* (1974) on sea ice in Resolute Bay, Northwest Territory, Canada. In these tests, the ice sheets were loaded by pumping water into large-diameter drums placed on them. The total loads and deflections at a few points were measured during the entire period of loading until breakthrough occurred. During the period of loading, many radial cracks formed first, followed by the formation of a few circumferential cracks prior to breakthrough.

Gold (1971) compiled data on the failure of floating ice sheets during logging and other operations. He presented the results of his survey in the form of two graphs: (1) a plot of load vs thickness associated with observed failure of ice covers, and (2) a similar plot associated with successful use of ice covers. He recommended that a good ice cover can safely support a load of $P = 1750h^2$, where P is the load in kilonewtons (kN) and h is the ice thickness in meters (m). He also noted that failures of ice covers were reported for loads as low as $P = 350h^2$ and as high as $P = 7000h^2$. He attributed the reasons for low bearing capacities of a floating ice cover to vehicle speed, thermal stress due to decrease in temperature, fatigue caused by repeated loading, and the quality of the ice cover. There is a need to supplement these data with other relevant information on load distribution, rate of loading, and ice temperature to understand the large scatter in the data.

Beltaos (1978) conducted a series of breakthrough tests by loading floating ice sheets for long periods of time. Using the results of his and others' tests, he proposed a failure criterion based on the concept of strain energy per unit volume. Using his empirical results on long-term loading tests, he recommended that a safe level of instantaneous loading on floating ice sheets is $P = 1790h^2$.

During the initial stages of loading, the deflections and stresses in a floating ice sheet can be obtained from axisymmetric, elastic analysis (Hertz, 1884; Wyman, 1950). The maximum tensile stress usually occurs in the center of the loading area on the top or bottom of an ice sheet for upward or downward loads, respectively. When the maximum tensile stress (Westergaard, 1926) equals the tensile strength of ice, radial cracks form from the loading area to a certain distance away. While the formation of radial cracks is an indication of high loads on a floating ice sheet, the breakthrough load is much higher than that which forms radial cracks. Although the middle surface of an ice sheet expands as a result of vertical deflections that cause separation between the vertical faces of the radial cracks, the bending action causes interference between the faces either at the top for downward loading or at the bottom for upward loading of an ice sheet. Hellan (1984) presented an axisymmetric elastic analysis of a plate with finite-size radial cracks and takes the above-mentioned interference into account. Recently, Dempsey *et al.* (1995) have presented an elastic analysis of radial cracking with closure for a circular, clamped plate (with no elastic foundation) loaded by a concentrated load at the center. Bazant *et al.* (1995) also discussed "the dome effect" caused by closure of radial cracks and presented some preliminary results of their analysis. Sodhi (1996) presented a deflection analysis of radially cracked, floating ice sheets by the finite element method. The results of this analysis were used to obtain the energy release rate (or the crack extension force) for radial cracks. The elastic energy release rate goes to zero when the radial cracks are about twice the characteristic length of a floating ice sheet. The length of radial cracks from this analysis are in agreement with those observed during full-scale and small-scale experiments.

An increase in load on a radially cracked ice sheet causes many circumferential cracks to form within a certain distance from the load (Frankenstein, 1963, 1966; Lichtenberger *et al.*, 1974). Despite the formation of radial and circumferential cracks, a floating ice sheet does not fail suddenly and remains capable of supporting vertical loads. This is only possible

because the fractured ice is surrounded by an intact ice sheet, which restrains the blocks from expansion and induces wedging action between them.

Sodhi (1995) obtained an estimate of the breakthrough load through a plastic limit analysis of the deforming region close to the load by assuming a velocity field and equating the rate of energy dissipation due to wedging (or compression) in the tangential and radial directions to the rate of work done by the load. In the range of ice thickness between 0.2 and 2.0 m, the agreement between the theoretical estimates and the experimental breakthrough loads is good, as long as energy dissipation due to radial deformation is ignored because of the formation of many circumferential cracks prior to breakthrough.

In this paper, we present the three approaches taken to obtain the load required to penetrate floating ice sheets. We conducted (1) plastic limit analysis of deforming region near the vertical load, (2) small-scale experiments to understand the wedging action during large deformation of ice sheets, and (3) full-scale measurements of ice penetration loads in the field. The overall objective is to validate the results of theoretical and small-scale experimental studies with full-scale measurements of ice penetration force.

2. ESTIMATION OF BREAKTHROUGH LOADS BY YIELD LINE METHOD

During the initial stages of loading of a floating ice sheet (i.e., small deflections), an area with a radius of 3–4 times the characteristic length is deflected vertically by the load. The characteristic length (l), which is obtained from the differential equation governing an elastic deflection of a floating ice sheet (Timoshenko and Woinowksy-Krieger, 1959), is the fourth root of the ratio of the flexural rigidity to the foundation modulus of an ice sheet. For freshwater ice, Gold (1971) suggested that $l = 16h^{3/4}$, where h is the ice thickness in m. The coefficient of $h^{3/4}$ depends on the elastic modulus of the ice, and it is estimated to be about 13.5 for sea ice. The radius at which vertical deflections are negligible is about 50–70 times the ice thickness.

When the maximum tensile stress due to elastic deformation in ice exceeds the tensile strength of ice, radial cracks form in the vicinity of the load. Observations made during field and laboratory experiments indicate that the large deflections during penetration or breakthrough are confined to a region close to the applied load, generally less than 10–20 times the ice thickness. This large deformation is superimposed on the large-area deflection described above. For sea ice, Lichtenberger *et al.* (1974) reported the initial formation of circumferential cracks at a distance of about 5–8 times the ice thickness from the edge of the distributed load. For freshwater ice, Frankenstein (1963, 1966) reported these distances to be in the range of 13–27 times the ice thickness. Both reported formation of more circumferential cracks of smaller radii as the deformation increased with the applied load. It is quite likely that such circumferential cracks also formed along the perimeter of the distributed load at the bottom of the ice sheet. As described later, many (5–10) circumferential cracks formed during small-scale experiments for the present study. The sequence of formation of these cracks was that the farthest one formed first, followed by other cracks closer to and around the area of load application.

Taking these observations into account, we first consider an axisymmetric formulation, which can be modified to consider other shapes of the loading area, to estimate the breakthrough load using plastic limit analysis. It is assumed that a total downward load P is distributed above an ice sheet over a circular area of radius a, as shown in Fig. 1. As the overall deformation proceeds, radial and circumferential cracks form, and the local deformation of ice takes place between radii a and b. It is assumed that the deformation takes place by formation of a continuous yield line field (Skrzpek, 1993) in the radial direction and that the resisting moment per unit length of a yield line is M_0. The following vertical velocity field ($\dot{w} \equiv dw/dt$) is assumed in terms of the vertical velocity ($\dot{w}_0$) at the load:

$$\dot{w} = \frac{b-r}{b-a}\dot{w}_0 \quad \text{for } a \leqslant r \leqslant b \tag{1}$$

where r is the radius of a point on the middle surface ($z = 0$) of the ice sheet. Figure 1

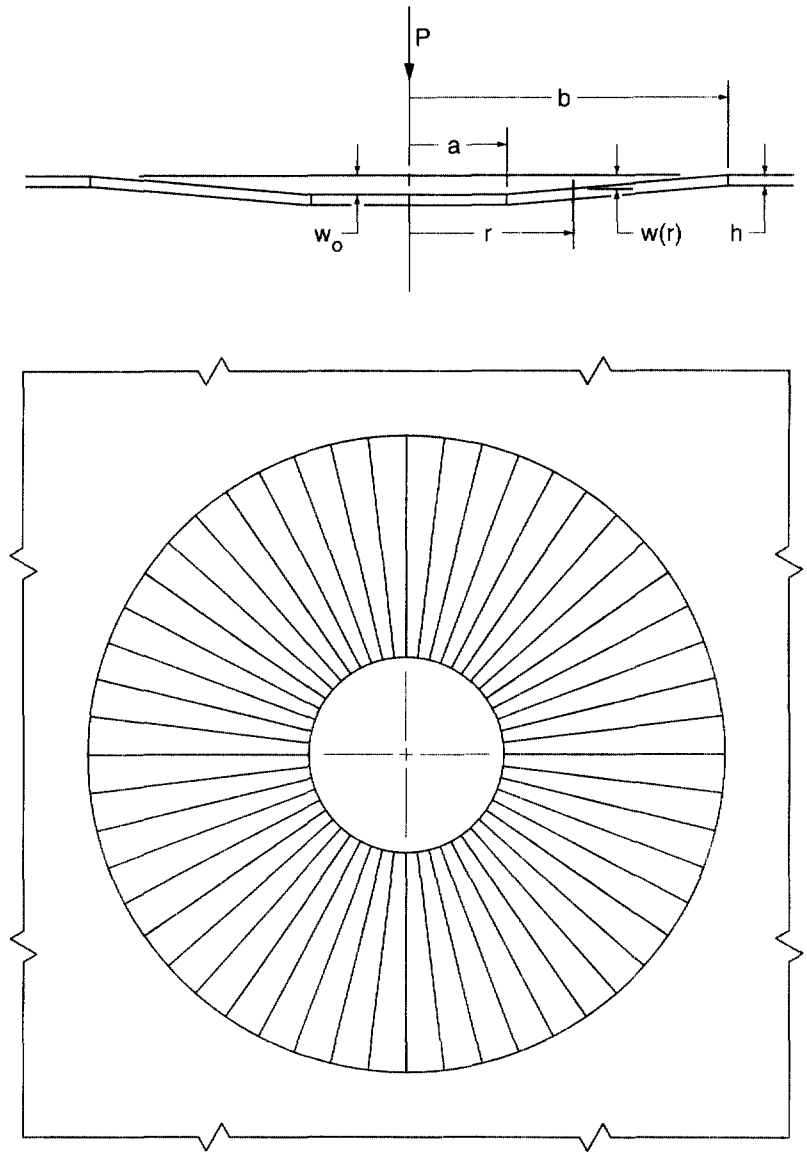

Fig. 1. Axisymmetric deformation of an ice sheet loaded over a circular area ($0 < r < a$).

shows a sketch of a deflected ice sheet at an instant in time with respect to radial distance r and vertical downward deflection w. Because the velocity $\dot{w}$ is zero at $r = b$, the assumed velocity field is relative to the velocity at $r = b$ from large-area deformation around the load. The rates of curvature change in the radial and tangential directions are given by:

$$\dot{\kappa}_{rr} = \frac{\mathrm{d}^2\dot{w}}{\mathrm{d}r^2} = 0 \quad \dot{\kappa}_{\theta\theta} = \frac{1}{r}\frac{\mathrm{d}\dot{w}}{\mathrm{d}r} = -\frac{1}{r}\frac{\dot{w}_0}{b-a} \tag{2}$$

Equating the rate of work done by the load P to the rate of energy dissipation in the deforming region of the ice sheet, we get:

$$P\dot{w}_0 = \int_0^{2\pi}\int_a^b (M_0|\dot{k}_{rr}| + M_0|\dot{k}_{\theta\theta}|)r\,\mathrm{d}r\,\mathrm{d}\theta + 2\pi(M_0|\dot{\Theta}_a a + M_0|\dot{\Theta}_b|b)$$

$$+\rho_w g\left(2\pi\int_a^b w\dot{w}r\,\mathrm{d}r + a^2 w_0\dot{w}_0\right), \tag{3}$$

where $\rho_w g$ is the specific weight of water, and $\dot{\Theta}_a$ and $\dot{\Theta}_b$ are the rates of change of slope discontinuities at $r = a$ and $r = b$, respectively. The first term is the rate of energy dissipation in the annular area between radii a and b, the second term accounts for the rate of energy dissipation along the circumferential cracks at radii a and b due to local deformation in the radial direction, and the third term is the rate of work done against buoyancy forces. Noting that $|\dot{\Theta}_a| = |\dot{\Theta}_b| = \dot{w}_0/(b-a)$, and substituting for the other variables in eqn (3) from eqns (1) and (2) we get:

$$P = 2\pi M_0 + 2\pi M_0 \frac{b+a}{b-a} + \frac{1}{6}\pi\rho_w g w_0 (b^2 + 2ab + 3a^2) \tag{4}$$

The third term, derived from the buoyancy forces, can be small in comparison to the first two terms under certain conditions. We can ignore it for the purpose of comparing the above result with the collapse loads of plates not supported on an elastic foundation (e.g., Skrzypek, 1993). The second term in eqn (4) accounts for the rate of energy dissipation because of interference between the rotating ice block and the adjoining ice sheet. It radius a is equal to zero, we get a collapse load [i.e., the first two terms in eqn (4)] $P = 4\pi M_0$, which is the same as the result for a concentrated load acting on a built-in (or fixed) plate at $r = b$ (Skryzpek, 1993). The second term becomes large when radius b is almost equal to radius a, which is a situation occurring during shear failure and not applicable to the estimation of failure load by eqn (4). During experiments done by Frankenstein (1963, 1966), shear failure occurred during concentrated load tests, and the breakthrough for a concentrated load occurred at a lower load than for a distributed load. Sodhi (1995) discussed the shear failure of an ice sheet and concluded that, if the load is distributed over a circular area with a diameter more than twice the ice thickness, the failure will take place in bending and not in shear. The holes made in the ice sheet during distributed load tests were always greater than the size of the loaded area. In other words, the radius b was greater than radius a by several ice thicknesses. If the interference at radii a and b is non-existent because of many circumferential cracks occurring in the ice sheet at $r > b$, the resisting moment along those circumferential cracks can be assumed to be zero, and we get a collapse load [i.e., the first term in eqn (4)] $P = 2\pi M_0$, which is the same as the result for a concentrated load acting on a simply supported plate at $r = b$ (Skryzypek, 1993). It is noteworthy that, for a simply supported boundary condition, we get the same collapse load for a distributed load acting on a circular area of radius a as that for a concentrated load and that the collapse load does not depend on radius b. This result is merely the result of plastic limit analysis under the assumed velocity field.

3. SMALL-SCALE EXPERIMENTAL STUDIES

3.1. *Setup and procedure*

We conducted all tests for this study with freshwater, columnar ice. We used wet seeding with small ice crystals to start the ice growth when the water and the ambient temperatures were 0 and -10°C, respectively. Seeding was done by spraying a mist of water with compressed air above the water surface in the basin. This result in fine ice crystals forming in the air and settling on the water surface. This process yields an ice sheet with small, uniform crystal sizes throughout the ice sheet. After seeding, we lowered the room temperature to -25°C for ice growth for a period of time to achieve the desired ice thickness. The resulting ice sheet had columnar structure with fine grains (1–2 mm) at the top and coarse grains (3–6 mm) at the bottom. The temperature of the ice at the time of testing was between -2 and 0°C.

To characterize an ice sheet, we measured its characteristic length and flexural strength. The characteristic length was measured by placing a dead load on a floating ice sheet and measuring the resulting elastic deflection with a displacement transducer (Sodhi *et al.*, 1982). The flexural strength was measured by pushing the tips of cantilever beams in the

upward and downward directions and measuring the maximum force and the size of broken beams (Ashton, 1986).

We conducted three types of beam tests and two types of plate tests by pushing the floating ice downward. We measured the reaction force during a test by a load cell as the ice was pushed down. The load cell was installed rigidly on the personnel carriage in the basin, which could be lowered at a constant velocity of about 4 mm s^{-1}. We measured the deflections at a few points with the help of displacement transducers.

To prepare beam and plates, we cut slots in the floating ice sheet with a chain saw, which was mounted on a platform that could be moved in the transverse direction on rails installed on the personnel carriage. To cut slots in the transverse direction, we moved the carriage to the desired location and moved the platform sideways by hand with the saw cutting the ice. To cut slots in the longitudinal direction of the basin, we positioned the saw at the desired location on the carriage and moved the carriage with the saw cutting the ice.

3.2. *Beam tests*

3.2.1. *Fixed-end beam tests.* Figure 2 shows the experimental setup to push down a beam with fixed ends. Two slots were cut in an ice sheet to create a beam of floating ice with its ends attached to the surrounding ice sheet. A vertical load was applied in the middle of the beam while measuring the deflections at one to three points along the beam.

Figure 3 shows a typical load-versus-deflection plot obtained from a fixed-end beam test. The load–deflection plot has a nearly constant slope during the initial stages of loading or deformation up to about 1.3 kN. Then there is a slight readjustment of load and deflection, indicating formation of vertical cracks during the test. After that, the slope of load–deflection plot continuously decreases with increase in deflection, indicating softening of the ice and/or a decrease in the wedging action. The vertical applied load reaches a maximum value before finally decreased to low values. In Table 1, we have listed the maximum loads recorded during all tests along with the length, width, and thickness of the fixed-end beams in each test.

After a test, we always observed two zones of microcracked ice in each of the two half-beams of ice, as shown in Fig. 4. These zones of microcracked ice formed in the top third of the thickness in the middle of the beam (where vertical load was applied), and in the bottom third of the thickness at the ends. We also observed horizontal cleavage cracks that formed in the middle and at the roots of fixed beams. In a few tests with thick (<80 mm) ice sheet, the cleavage cracks at the root extended a long distance (≈ 0.1–0.2 m) into the ice and occurred at about one-third of the ice thickness from the bottom. In tests with thin (>80 mm) ice sheets, cleavage cracks propagated a short distance (≈ 0.05–0.06 m), as indicated by small protrusions of ice at the sides of blocks in the bottom third of their

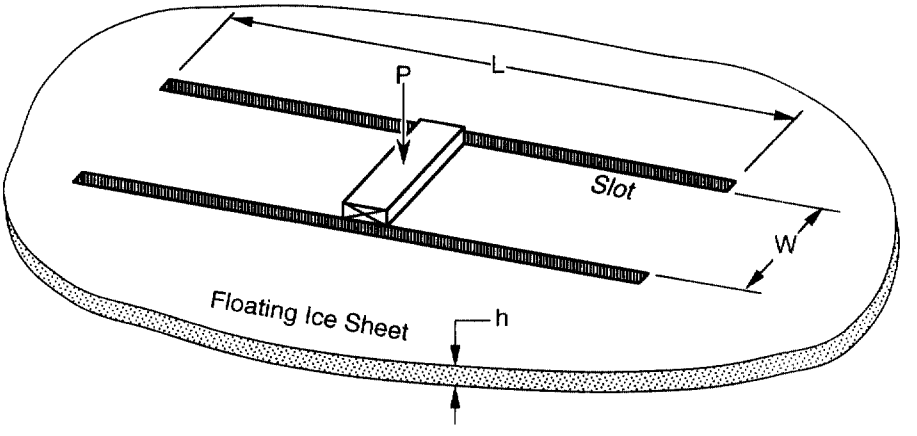

Fig. 2. Experimental setup to push down a beam with fixed ends.

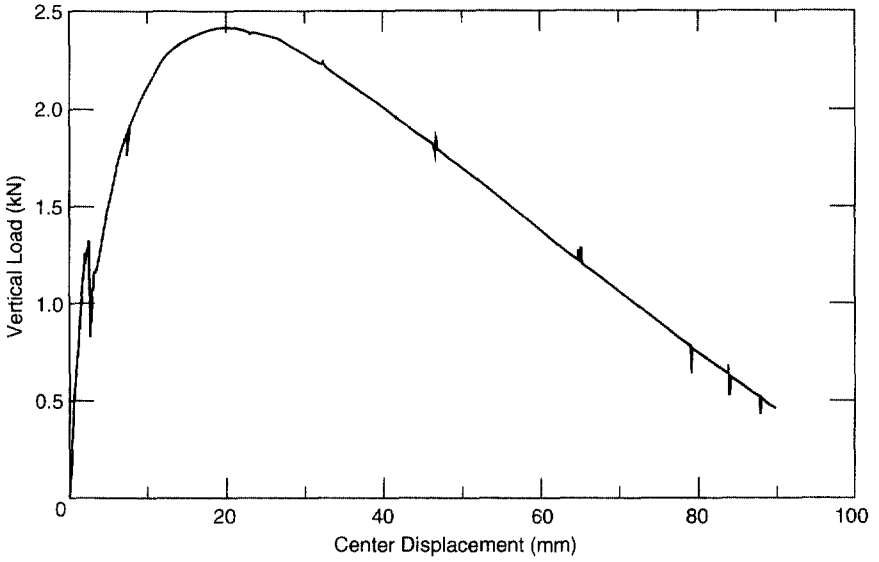

Fig. 3. Plot of load vs deflection from a fixed-end beam test (S-8).

Table 1. Beam dimensions and maximum wedging pressure during fixed-end beam tests

Date	Test number	L (mm)	w (mm)	h (mm)	Max. wedging pressure (MPa)
09/14/94	S-4	2083	298	114	2.747
09/15/94	S-8	3060	298	117	2.367
09/15/94	S-10	8079	295	114	2.302
09/15/94	S-12	5000	300	114	2.261
09/22/94	S-16	1570	298	148	3.173
09/22/94	S-17	3000	292	147	2.387
09/22/94	S-20	2000	290	147	2.257
09/28/94	S-23	1500	418	121	3.254
09/28/94	S-26	1500	292	120	3.347
09/29/94	S-29	2030	297	127	2.831
09/29/94	S-30	2510	290	127	2.911
09/29/94	S-31	3050	298	132	2.522
09/29/94	S-32	1540	296	131	2.649
10/03/94	S-35	985	284	83	2.642
10/03/94	S-36	2350	276	82	3.116
10/07/94	S-42	752	296	89	2.765
10/07/94	S-43	1480	302	92	2.609
10/07/94	S-44	1900	302	91	2.999
10/07/94	S-45	978	298	92	2.373
10/11/94	S-50	500	290	69	2.759
10/11/94	S-51	750	283	70	3.031
10/11/94	S-52	1000	287	69	3.268
10/11/94	S-53	1500	285	71	3.018
10/11/94	S-54	2000	295	68	3.157
10/14/94	S-61	735	287	68	3.136
10/14/94	S-62	920	312	67	2.922
10/14/94	S-63	1470	297	68	2.819
10/14/94	S-64	1975	288	66	2.952

thickness. We also observed zones of microcracked ice and three or four vertical macrocracks fanning out into the adjacent ice from the ends of a beam, indicating that the ice was compressed by the ends of the beam. At times we also observed vertical cracks running along the length of a beam.

3.2.2. *Cantilever beam tests.* In a few tests, we cut a slot in the middle of a fixed-end beam, effectively creating a pair of cantilever beams. When a load was applied in a similar

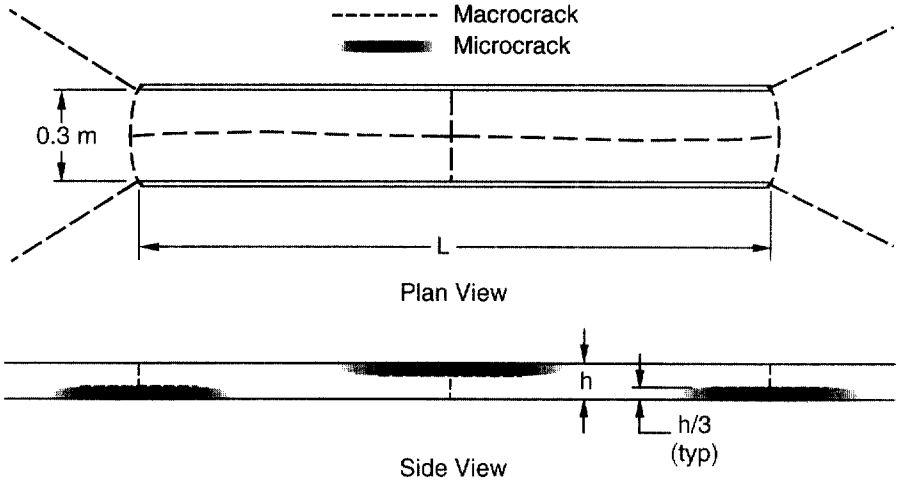

Fig. 4. Zones of microcracked ice in blocks after a fixed-end beam test.

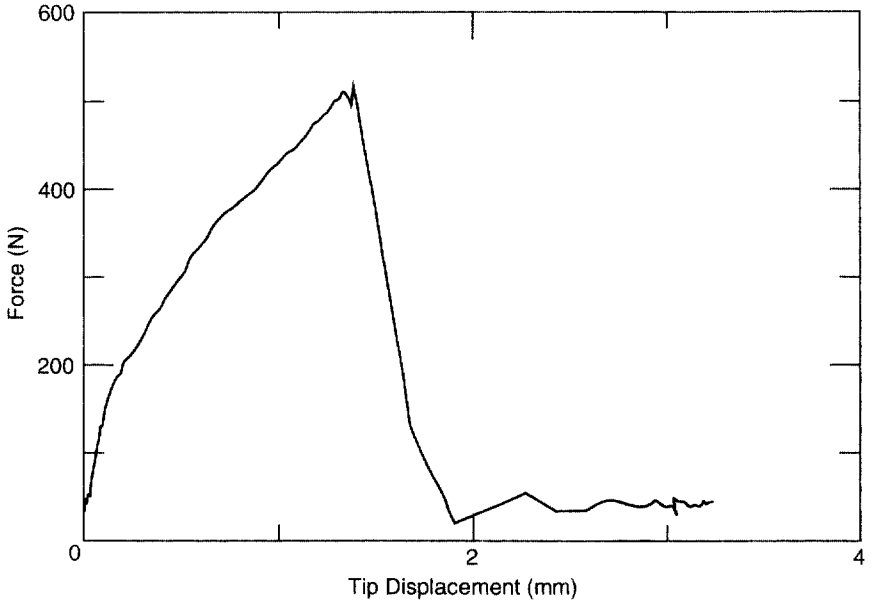

Fig. 5. Plot of load vs tip deflection from a cantilever beam test in which L_{arc} = 486 mm, w = 303 mm, h = 70.5 mm.

manner as for a fixed-end beam, the slot in the middle prevented the development of any in-plane force, and the cantilever beams failed in bending at the roots. As shown in Fig. 5, the load increases almost linearly with respect to tip deflection, until the ice fails by fracture at the roots. We did not observe any zone of microcracking in the broken pieces of the two cantilever beams. The failure load in these tests was much lower than that for a similar size beam with fixed ends.

3.2.3. *Measurement of in-plane forces in beam tests.* To measure in-plane forces, we inserted an apparatus between the opposed ends of two cantilever ice beams, and pushed down at a constant velocity until failure took place. Figure 6 shows the experimental setup and the apparatus, which consisted of two steel plates with three load cells between them. The apparatus was suspended with flexible strings (bungee cords) from a crane. We lowered the apparatus slowly into the slot between the ends of the beams, so that the plates did not touch the ends of the beams. When the plates were aligned with respect to the beams, the

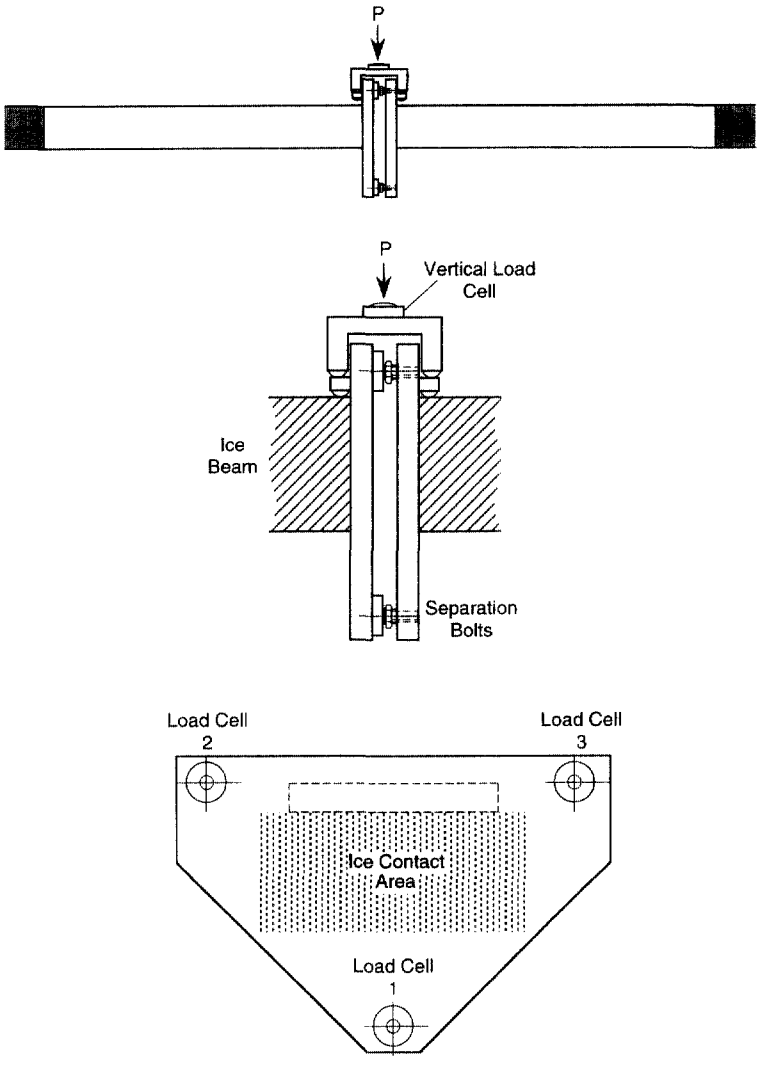

Fig. 6. Experimental setup to measure in-plane forces with an apparatus inserted between two cantilever beams.

hexagonal bolts in the plates were tightened to separate the plates against the ends of the beams. When the forces, as indicated by the three load cells between the plates, were approximately equal, we allowed the ice to creep and reduce the preload forces, so as to make good contact with the steel plates. When the load on the ends of the beams had relaxed to a low value, the test was conducted with the apparatus pushed down at a constant velocity.

Figure 7 shows typical plots of the vertical load, the forces as measured by three load cells, and the in-plane force (i.e., sum of forces measured by three load cells) with respect to center displacement. Comparing the load–deflection plots of vertical loads in Figs 2 and 7, it can be seen that the plot of vertical force has similar characteristics as that for fixed-end beam tests. As shown in Fig. 7, the in-plane force and the vertical force reach their maximum values at different displacements or times. An analysis of these data will be presented later. In Table 2, we have listed the maximum load and the size of beams used for this type of test.

3.3. *Plate tests*

We pushed down the center of floating ice sheets at a constant velocity of about 4 mm s^{-1} while measuring the vertical load and the deflections at three points. We applied the

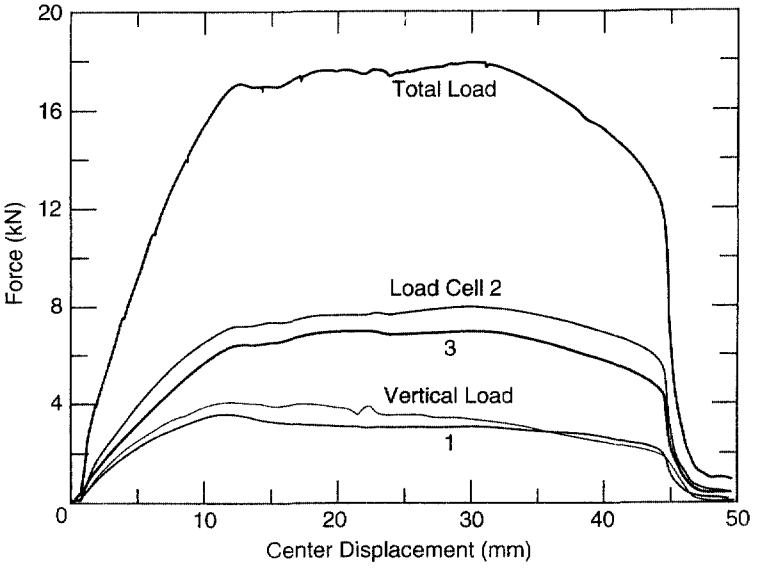

Fig. 7. Plots of vertical load, forces measured by load cells, and total in-plane force with respect to center displacement (S-27).

load by placing a 406 mm diameter disk of 9 mm thick plywood on top of an ice sheet. In a few tests, we applied the load using a 152 mm diameter disk. To determine breakthrough loads of the floating ice sheets with and without wedging action, tests were performed with two types of boundary conditions on the edges of the ice sheets as described below. We did not observe any flooding near the load prior to breakthrough.

To simulate an infinite ice sheet in small-scale tests, the extent of a floating ice sheet should at least be about 8–10 times the characteristic length. The width of the model basin at CRREL is about 9.15 m, and does not satisfy this requirement during most tests in this study. Though the proximity of basin walls may have influenced the overall deformation of floating ice sheets, it did not influence the large deformation and fracture pattern in the vicinity of load. In this study, the breakthrough load is assumed to depend on the load carrying capacity of the ice sheet in the vicinity of the load, and is, therefore, unaffected by the proximity of the basin walls.

3.3.1. *Fixed floating ice sheet.* When we pushed down an ice sheet attached to the basin walls, we observed many ($\approx$20–30) radial cracks forming around the load shortly after the start of a test. Some (6–10) of the radial cracks propagated farther from the load than others. As the test continued, we observed that many (5–10) circumferential cracks formed around the load. The sequence of circumferential crack formation was that the first crack formed farthest from the load, followed by others closer to the load, until the breakthrough occurred. We also observed interlacing microcracks over large areas between radial cracks at a distance of about 1–2 m from the center of the load. We believe that this microcracking formed as a result of compression of the ice in the tangential direction.

Figure 8 shows a typical load-versus-deflection plot from tests with an ice sheet fixed to the basin walls. During the initial stages of loading, the vertical force increases almost linearly with deflection (up to about 4.5 kN) until radial cracks form, at which point a slight unloading takes place, as indicated in the plot. After the formation of radial cracks, the load–deflection plot has a few sudden unloadings, indicating the formation of circumferential cracks. The slope of the load–deflection plot decreases continuously until the load reaches a maximum value, and then continues to decrease gradually until breakthrough takes place with a sudden drop in load to low values. The load–deflection plot is similar to that of the fixed-end beam tests, except during the period of unloading. This indicates that a similar process (i.e., compression of ice) governs the overall failure of a floating ice sheet.

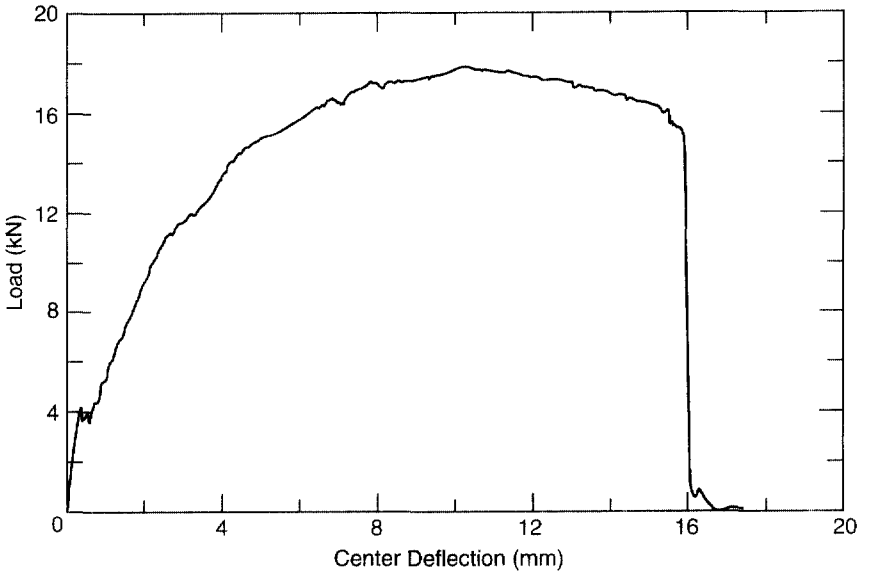

Fig. 8. Plot of load vs center deflection from a fixed-edge floating ice sheet test (S-47).

Table 2. Beam dimensions during beam tests with apparatus inserted between ends of two cantilever beams

Date	Test number	L (mm)	w (mm)	h (mm)
09/14/94	S-05	2003	280	113.0
09/15/94	S-09	2991	290	113.5
09/22/94	S-21	2000	293	146.0
09/28/94	S-27	1500	288	125.5
09/28/94	S-28	2000	296	131.0

Table 3. Ice thickness (h), maximum load (P), and nominal stress ($P/h2$) during fixed ice sheet tests

Date	Test number	h (mm)	P (kN)	$P/h2$ (kPa)
09/01/94	F-40	59	6.960	1999
09/01/94	F-41	59	6.568	1887
09/09/94	F-60	63	7.421	1870
09/09/94	F-61	63	7.149	1801
10/03/94	S-37	80	13.541	2116
10/03/94	S-38	72	10.844	2092
10/07/94	S-47	95	17.871	1980
10/11/94	S-56	69	9.086	1908
10/11/94	S-57	68	8.171	1767
10/14/94	S-66	66	9.600	2204
10/14/94	S-67	65	6.971	1650

In Table 3, we have listed the maximum values of the loads recorded during all tests of this type, along with the ice thicknesses.

3.3.2. *Free floating ice sheet.* In a portion of an ice sheet, we cut slots around an 8 m wide and 9 m long area, so that it was free on all sides. When we pushed down in the centre of the separated ice sheet, we observed that five to seven radial cracks form and propagate slowly to the edge of the ice sheet. During the first three tests, the width of the slots cut around the ice sheet was as wide as the width of the chain saw. When we observed that the failure took place by formation of straight circumferential cracks around the load, forming

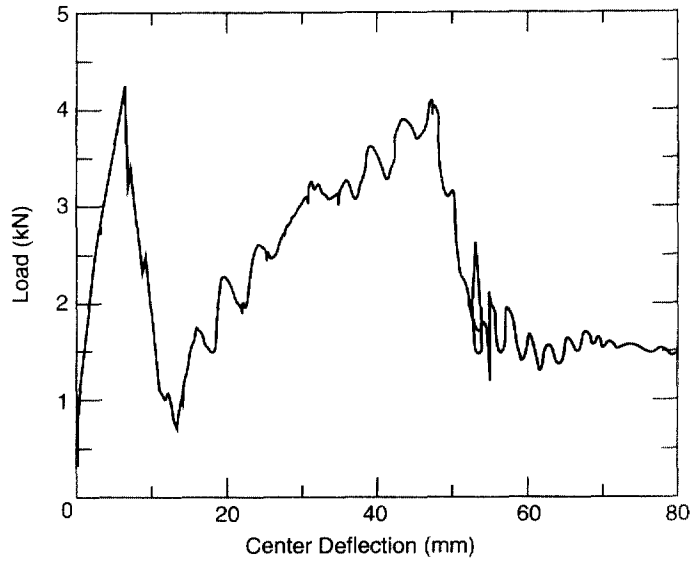

Fig. 9. Plot of load vs center deflection from a free-edge ice sheet test (S-46).

Table 4. Ice thickness (h), maximum load (P), and nominal stress ($P/h2$) during free ice sheet tests

Date	Test number	h (mm)	P (kN)	$P/h2$ (kPa)
09/01/94	F-39	60	4.905	1362
09/09/94	F-59	64	2.280	557
10/03/94	S-39	80	7.860	1228
10/07/94	S-46	93	4.206	486
10/11/94	S-55	68	4.114	890
10/14/94	S-65	65	2.686	636

a closed polygon, we suspected that the surrounding ice sheet may have restrained the separated plate of ice from expansion, because the slots were not wide enough to avoid interaction at the edges. Therefore, in the last three tests, we cut a wider slot to eliminate any chances of restraint from the surrounding ice. We observed that the failure during these last three tests took place when the radial cracks reached the boundaries, and the tips of a few wedge-shaped ice pieces broke at the time of failure. We did not observe any micro-cracking in any portion of the ice sheet after these tests. We observed a little flooding near the load prior to breakthrough.

Figure 9 shows a typical load-versus-deflection plot from tests with an ice sheet free on all sides. In contrast to the loading of a fixed ice sheet, the load in Fig. 9 increases linearly until radial cracks form, resulting in sudden unloading and increased deflection. After formation of radial cracks, the load increases again linearly with the increase in deflection until the cracks reach the boundary. In Table 4, we have listed the maximum loads recorded during these tests, along with the ice thicknesses. It should be noted that the magnitude of loads at which radial cracks begin to form were about the same for fixed and free boundary conditions, as shown in Figs 8 and 9.

3.4. *Discussion*

In the following, we analyze the experimental results of the beam and plate tests to estimate the breakthrough loads of floating ice sheets. Based on observations made during the beam tests, we propose a simple model to obtain data on the wedging pressure that develops between the ice blocks during the tests. These data are used in a theoretical model, based on plastic limit analysis, to predict the breakthrough loads of floating ice sheets.

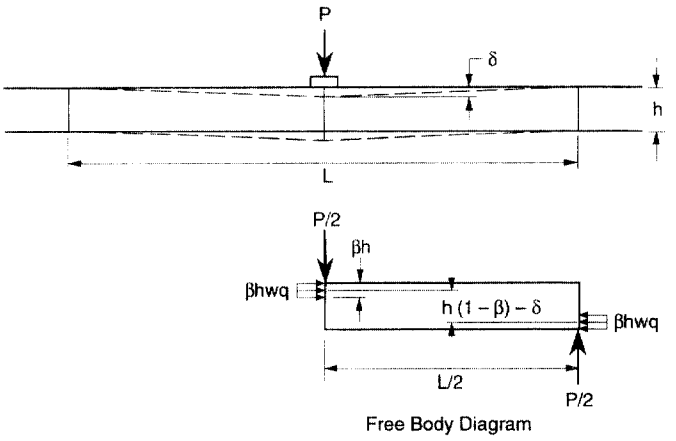

Fig. 10. Diagram of forces acting on one ice block during a fixed-end beam test.

These predictions are then compared with those obtained from fixed floating ice sheet tests and other full-scale tests. The validity of scaling laws, as proposed by Slepyan (1990) and Bazant (1993), for the breakthrough loads of floating ice sheets is also discussed.

3.4.1. *Beam test results.* Peters *et al.* (1982) considered the collapse of a built-in (fixed-end) beam that is loaded in the middle and restrained from expansion. They assumed that three plastic hinges, two at the support and one in the middle of the beam, develop resisting moments through eccentric compressive stresses in a section while ignoring the tensile stresses.

After fixed-end beam tests, we observed microcracking of ice in zones within each block in the middle and at the ends of a beam, as shown in Fig. 3. These zones of microcracking form as a result of wedging pressure acting in the horizontal direction on the faces of vertical cracks that form during the initial stages of deformation or loading. Based on this observation, we assume that a uniform pressure q acts uniformly across the beam width w and a portion of ice thickness βh at the top and at the bottom of each block, when a vertical force P acts in the middle of a beam of length L, as shown in Fig. 10. Considering the equilibrium of the forces acting on each block, we get the following equation for the wedging pressure q from the moment balance about the center of each block:

$$q = \frac{PL}{4wh^2\beta(1-\beta-\delta/h)}, \tag{5}$$

where δ is the relative displacement of the beam center with respect to its ends. It should be noted that this equation is not valid for large deflections when the denominator approaches zero.

As described earlier, we conducted five successful tests by installing an apparatus between the slots cut in the middle of fixed-end beams to measure the magnitudes of the in-plane forces caused by the wedging action. Assuming $\beta = 1/3$, we get a direct measurement of wedging pressure by dividing the total in-plane force by the assumed contact area ($wh/3$). To compute the wedging pressure using eqn (5), we used the data on beam dimensions listed in Table 2. The relative displacement of δ is obtained by subtracting the measured displacement at one end of a fixed-end beam from that at the center. A comparison of wedging pressure obtained from measured in-plane forces and that computed from eqn (5) is shown in Fig. 11. Considering the difficulties encountered during direct measurement of in-plane forces, the comparison is good. This comparison validates estimation of wedging pressure q from eqn (5).

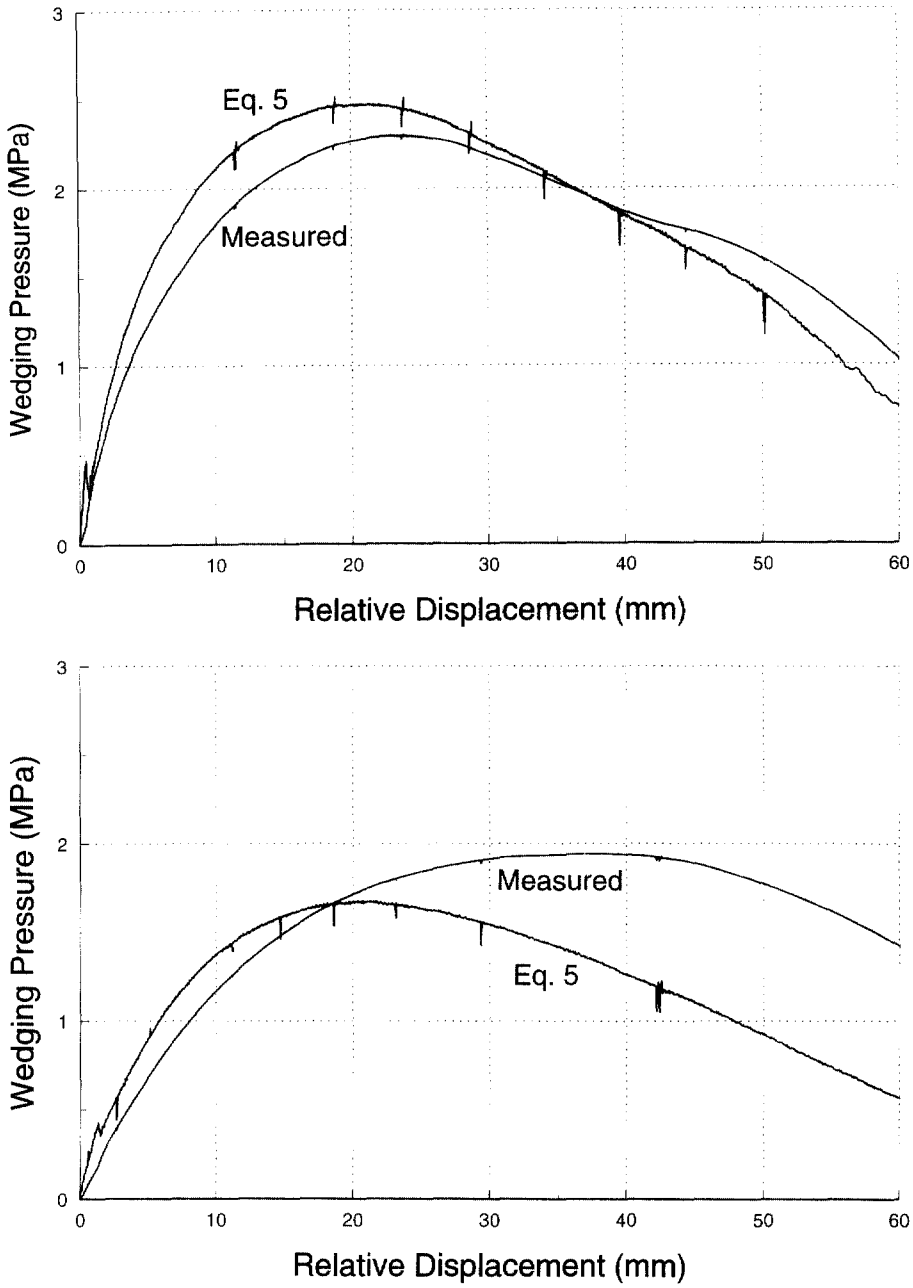

Fig. 11. Plots of wedging pressure from measured in-plane force and eqn (5) with respect to center displacement: (a) Test S-5, (b) Test S-9, (c) Test S-21, (d) Test S-27, and (e) Test S-28.

For $\beta = 1/3$, we have listed the maximum values of the wedging pressure q in Table 1 corresponding to the maximum values of the vertical loads and other beam dimensions during the fixed-end beam tests. Figure 12 shows a plot of the maximum wedging pressure q with respect to beam length L listed in Table 1. If the strain or strain rate caused by the wedging action depended on the beam length, we could expect a decrease in wedging pressure ($\propto L^{-1}$ or $L^{-1/2}$) with an increase in beam length. There is some scatter in the plot of q vs L, but there appears to be no dependence of wedging pressure q on the beam length. It appears that the wedging pressure that develops on the edges of each block is caused by local deformation of ice within each block. The wedging pressure q has a range between 2.257 and 3.437 MPa, and its mean and standard deviation are 2.809 and 0.336 MPa, respectively.

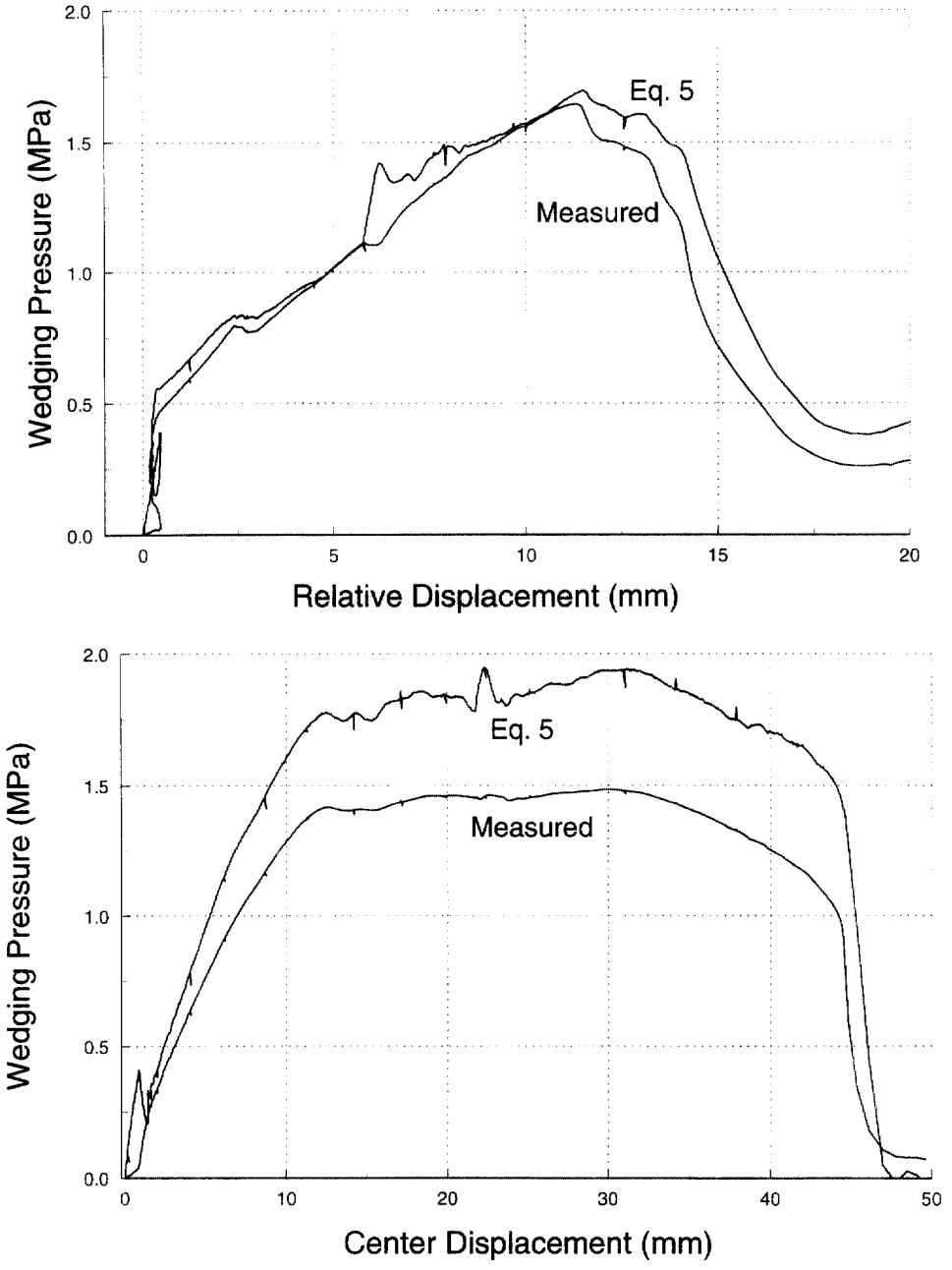

Fig. 11—*Continued.*

If the rotation takes place at the centre of a beam, the resisting moment per unit width of an ice sheet is given by $M_0 = qh^2\beta(1-\beta)/2$. Using a value of $\beta = 1/3$, we get an $M_0 = qh^2/9$. The resisting moment per unit length calculated from flexural strength is given by $M_f = \sigma_f h^2/6$ or $M_f = \sigma_f h^2/4$ (Meyerhof, 1960), where σ_f is the flexural strength of ice. An average value of σ_f obtained from downward and upward flexural strength tests was about 0.75 MPa. Taking the mean value $\sigma = 2.81$ MPa, we get a ratio of $M_0/M_f \approx 2.5$, which is lower than that predicted by Peters *et al.* (1982). This may be attributed partly to the warm ice as used in tests during this study.

Cantilever beam tests were done to demonstrate that the vertical forces to cause flexural failure in similar size beams are lower than those that cause failure with wedging action. The results of the cantilever beam tests may be used to predict the loads at which vertical cracks form during the initial stages of fixed-end beam deformation or loading. Estimates

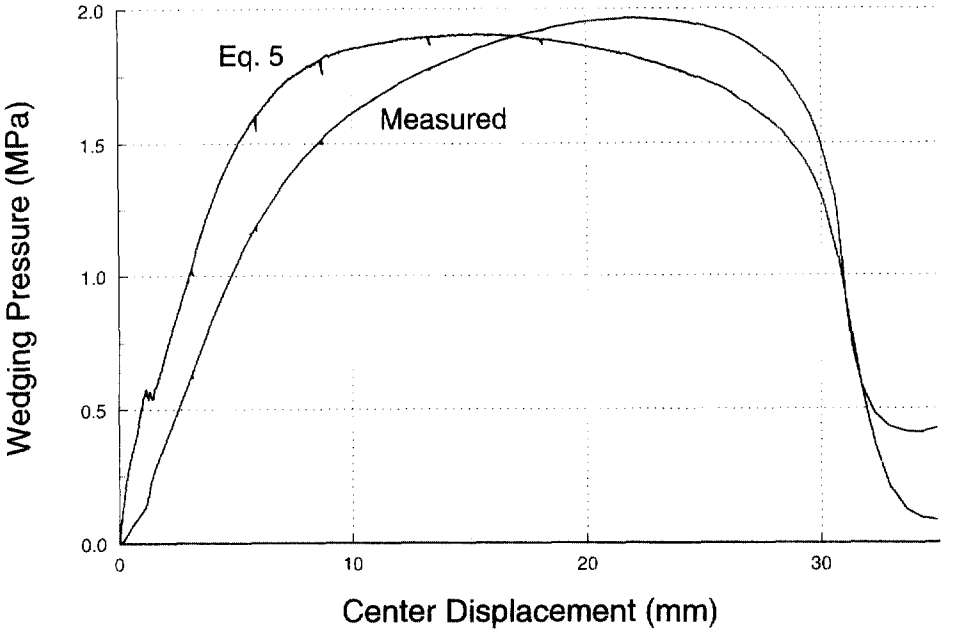

Fig. 11—*Continued.*

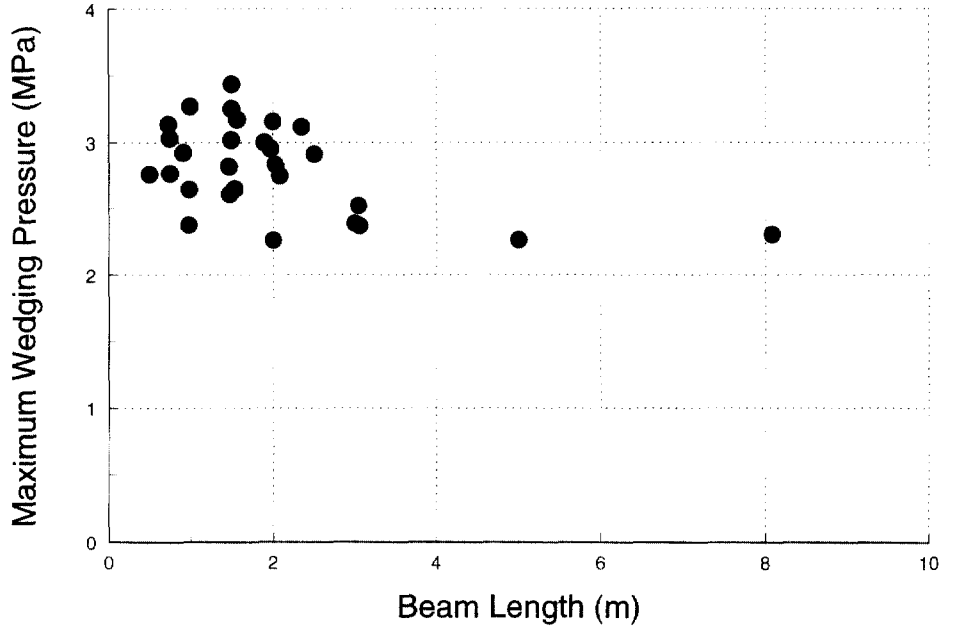

Fig. 12. Plot of maximum wedging pressure with respect to beam length.

of loads based on elastic analysis (Wyman, 1950) and flexural strength for the prediction of the load to form the first crack in a sheet agree reasonably well with those measured in this study.

3.4.2. *Plate tests results.* The maximum vertical loads recorded during plate tests with fixed and free boundary conditions are given in Tables 3 and 4. The breakthrough loads

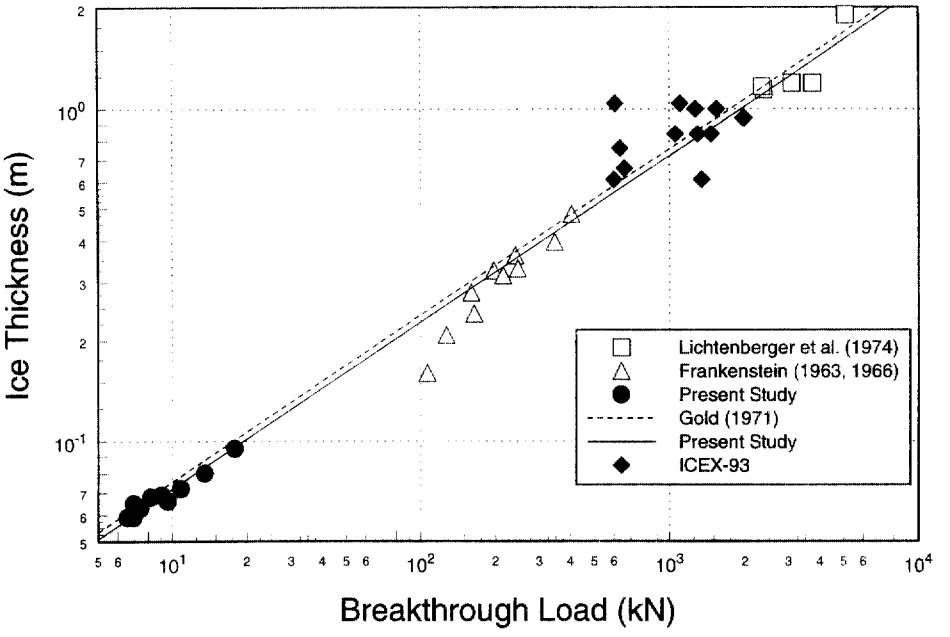

Fig. 13. Plot of breakthrough load vs ice thickness; two lines are plots of $P = 1750h^2$ (Gold, 1971) and $P = 1934h^2$ (present study).

from the fixed ice sheet tests (Table 3) are plotted with respect to ice thickness in Fig. 13, where the data from full-scale tests (Frankenstein 1963, 1966; Lichtenberger *et al.*, 1974) are also shown.

To compare these data with data from other sources, the breakthrough load is divided by the square of the ice thickness to obtain a nominal stress (or empirical factor) α in kilopascals (kPa). In the present study, the range of α is between 1650 and 2204 kPa for the fixed ice sheets, and the mean and standard deviation are 1934 and 164 kPa, respectively. Mean and standard deviation of α from the free ice sheet tests are 860 and 366 kPa, respectively. The mean value of α for the free ice sheets is less than half of that for the fixed ice sheets, but the standard deviation of α for fixed ice sheets is less than that for free ice sheets. The higher standard deviation for free ice sheets can perhaps be attributed to the confinement offered by surrounding ice during the first three tests. The reason for the difference in the mean values of α may be attributed to the difference in constraint provided by the boundaries of fixed and free ice sheets. After formation of radial cracks during loading of a free ice sheet, the cracks propagate to the boundary upon further loading, and the ice sheet disintegrates into pieces and is thereby unable to carry any load. In contrast, the radial cracks in a fixed ice sheet do not propagate any further after their formation, and the wedges formed by radial cracking push against each other in response to further loading of an ice sheet. The existence of wedging action in fixed ice sheets is the main reason that its load-carrying capacity is higher than that for free ice sheets. The two lines in Fig. 13 are plots of $P = 1750h^2$ (Gold, 1971) and $P = 1934h^2$, obtained from the results of fixed ice sheet tests.

As discussed earlier, the estimates of the collapse load according to plastic limit analysis for the following boundary conditions are: $P = 2\pi M_0$ for a simply supported boundary condition at the edge of the plate, and $P \approx 4\pi M_0$ for a fixed or built-in boundary condition. Recalling that $M_0 = qh^2/9$ and the mean value of q is 2.4 MPa for the ice used in the present study, we get $P = 1962h^2$ for the simply supported boundary condition, and $P = 3924h^2$ for the fixed or built-in boundary condition. It should be noted that the value of $\alpha = 1962$ kPa is close to the mean value of $\alpha = 1934$ kPa obtained from small-scale tests in this study. The estimated collapse load for the simply supported boundary condition is close to the breakthrough load obtained from the full-scale and small-scale tests. Moreover, the

formation of many circumferential cracks also supports the assumption of the simply supported boundary condition, as discussed by Sodhi (1995).

The results of this study show that it is possible to predict the breakthrough load of a floating ice sheet by conducting a few fixed-end beam tests and measuring the relative displacement δ and the applied load to cause failure of the beam. Using eqn (5), we can determine the maximum wedging pressure q that ice can resist, and the maximum resisting moment ($M_0 = qh^2/9$) per unit length. Using the results of plastic limit analysis, we can then predict the breakthrough load for the simply supported boundary condition, i.e., $P = 2\pi M_0$.

Though the plots of breakthrough load vs ice thickness in Fig. 13 from the field tests and the small-scale tests appear to have the same trend, there are three factors that need to be considered: (1) rate of loading, (2) salinity, and (3) ice temperature. These parameters affect the creep properties of ice. The rate at which the ice sheet moved near the area of loading during field tests is about 0.1 mm s^{-1}, whereas it was 4 mm s^{-1} during small-scale tests. The ice temperature during small-scale tests was about -1°C, whereas it was in the range of -10 and 0°C. All small-scale tests were done with freshwater ice, whereas one series of field tests was done on sea ice. Though the effect of these factors on the breakthrough load need further investigation, we believe that their effects are secondary to those of ice thickness (Sodhi, 1995).

3.4.3. *Scaling laws.* Slepyan (1990) and Bazant and Li (1994) investigated the size effect of a radially cracked floating ice sheet. For the propagation of radial cracks, they found that the nominal stress (load divided by the square of ice thickness P/h^2) is proportional to (ice thickness)$^{-3.8}$, or equivalent to (characteristic length)$^{-1/2}$. However they did not find any size effect for the maximum load, because this load is assumed to occur at the initiation of circumferential cracks, which is governed by a strength criterion. In discussing the scaling laws in the mechanics of failure, Bazant (1993) concluded that the nominal strength of a structure is independent of its size when the failure condition is expressed in terms of stress or strain only, including elasticity with strength limit, plasticity, and continuum damage mechanics. When the failure condition involves both stress and energy per unit area (e.g. for fracture), the scaling law represents a gradual transition from the strength theory, i.e., (size)^0, to linear elastic fracture mechanics, i.e., (size)$^{-1/2}$. According to observations made during full-scale and small-scale experiments, the breakthrough does not take place immediately after the formation of circumferential cracks, because of wedging action between radially cracked ice sheets. Sodhi (1995) has presented a theoretical model in which the work done by the load causes dissipation of energy in compressing ice in the tangential direction. Because the nominal stress (P/h^2) depends on the compression strength of ice, there is no scale effect. This is also supported by the results of full-scale and small-scale experiments, as shown in Fig. 13.

4. FULL-SCALE MEASUREMENTS

We used a methodology based on the Archimedean principle to measure the ice penetration force during the ICEX-93 program (Dane, 1993). When a short-term force is applied to a floating ice sheet, the force is equal to the weight of water displaced as a result of local deformation of the ice sheet around the load (Ashton, 1986). The measurement of uplifting force can then be accomplished by measuring the vertical deflections at a few points along a radial line in the vicinity of the load and then obtaining the volume of the displaced water. We verified this methodology in the laboratory (Sodhi, 1989) before using it in the field.

During the ICEX-93 program, we measured the vertical deflections with the help of pressure transducers installed at a few points along two separate tubes filled with a solution of glycol, as shown in Fig. 14. We analyzed the data from pressure transducers to obtain plots of the vertical displacement vs radial distances from the sail. We assumed an axisymmetric displacement of the ice sheet around the sail and integrated the plots of displacement vs radial distance to obtain the volume and the weight of displaced water, which

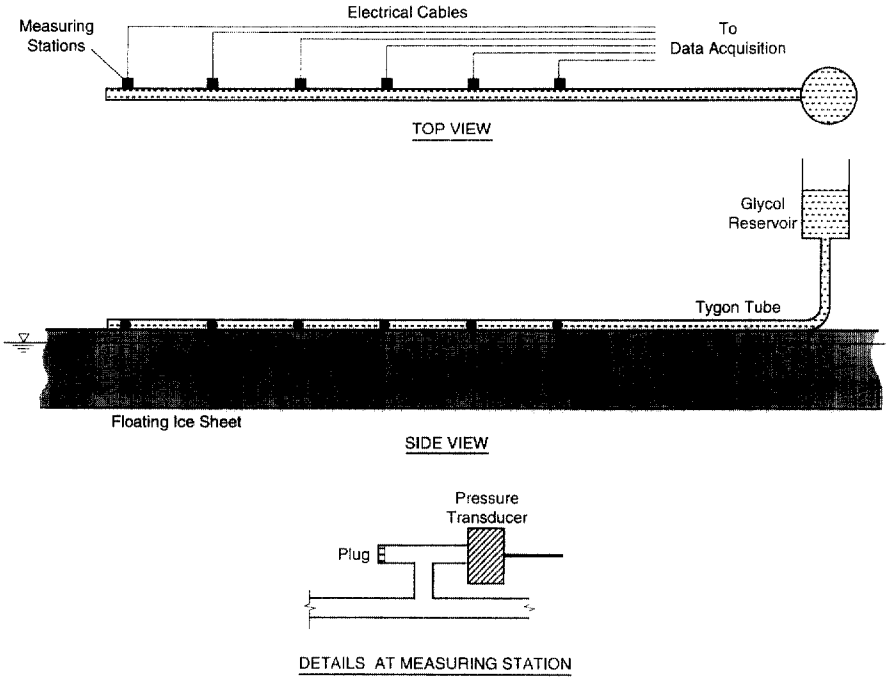

Fig. 14. Pressure transducers and glycol-filled tube to measure vertical displacement of a floating ice sheet.

is equal to the force during uplifting of a floating ice sheet, at each scan of the data. The maximum force in the plot of uplifting force is taken to be the ice penetration force. Figure 13 shows plots of the ice penetration force vs ice thickness from the ICEX-93 field program. The ICEX-93 data lie close to the lines obtained from theoretical and small-scale experimental results and the empirical relationship proposed by Gold (1971). However, there is a large scatter in the data because of errors incorporated in the field measurement.

5. CONCLUSION

We took three approaches to determine the force required to penetrate a floating ice sheet: (1) plastic limit analysis, (2) small-scale experiments, and (3) full-scale measurements in the field. During the vertical loading of a floating ice sheet, radial and circumferential cracks form as a result of deformation in the ice. Despite these cracks, the ice sheet is able to support a load because the cracked ice is surrounded by intact ice, and further deformation in the ice is resisted by the development of in-plane wedging pressure in the top or bottom portions of an ice sheet. A series of beam and plate tests was conducted in the laboratory to understand the wedging action. The data from the beam tests reveal that compressive stresses develop in the top or bottom third of the ice thickness to resist deformation. This model is validated by direct measurement of in-plane forces by inserting an apparatus between the opposed free ends of two cantilever beams. The wedging pressures obtained from the measured in-plane force agree well with those obtained from the equilibrium of each block. Breakthrough loads of fixed ice sheets were about twice those obtained from tests with ice plates having free boundary conditions. This difference is attributed to the wedging action that is caused by the restraint imposed by the surrounding ice sheet on the fracture scale in the vicinity of the load. Data from the beam tests are also used to predict the breakthrough loads of floating ice sheets, and these predictions compare well with the breakthrough loads obtained from small-scale and full-scale tests on floating ice sheets.

Acknowledgements—This work is supported by funding from the In-house Laboratory Independent Research Program at the U.S. Army Cold Regions Research and Engineering Laboratory, Hanover, New Hampshire, and

the Carderock Division, Naval Surface Warfare Center, Bethesda, Maryland. The author gratefully acknowledges the help of Jesse M. Stanley in conducting the small-scale experiments and in measuring the full-scale ice penetration forces in the field. The author thanks the reviewers of this paper for their suggestions to improve the paper.

REFERENCES

Ashton, G. D. (1986) *River and Lake Ice Engineering*. Water Resources Publication, Littleton, Colorado.

Bazant, Z. P. (1993) Scaling laws in mechanics of failure. *ASCE Journal of Engineering Mechanics* **119**(9), 1828–1844.

Bazant, Z. P. and Li, Y.-N. (1994) Penetration fracture of sea ice plate: simplified analysis and size effect. *ASCE Journal of Engineering Mechanics* **120**(6), 1304–1321.

Bazant, Z. P., Kim, J. J. H. and Li, Y.-N. (1995) Part-through bending cracks in sea ice plates: mathematical modeling. *Ice Mechanics*—1995, ed. by J. P. Dempsey and Y. D. S. Rajapakse, AMD-Vol. 207, pp. 97–106. American Society of Mechanical Engineers, New York.

Beltaos, S. (1978) A strain energy criterion for failure of floating ice sheets. *Canadian Journal of Civil Engineering* **5**, 352–361.

Beltaos, S. and Lipsett, A. W. (1979) An empirical analysis of the floating ice sheets. *Proceedings, Workshop on the Bearing Capacity of Ice Covers*, pp. 124–136. Winnipeg, Manitoba, Canada, National Research Council of Canada, Technical Memorandum No. 123, pp. 124–136.

Dane, A. (1993) Ice Station X. *Popular Mechanics* **170**(11), 30–34, 132.

Dempsey, J. P. Slepyan, L. I. and Shekhtman, I. I. (1995) Radial cracking with closure. *International Journal of Fracture* **73**, 1–36.

Frankenstein, G. E. (1963) Load test data for lake ice sheets. Technical Report 89, U.S. Army Cold Regions Research and Engineering Laboratory, Hanover, New Hampshire.

Frankenstein, G. E. (1966) Strength of ice sheets. In *Proceedings, Conference on Ice Pressures against Structures*, pp. 79–87. Laval University, Quebec, National Research Council of Canada, Technical Memorandum No. 92, NRCC No. 9851.

Gold, L. W. (1971) Use of ice covers for transportation. *Canadian Geotechnical Journal* **8**, 170–181.

Hellan, K. (1984) An asymptotic study of slow radial cracking. *Int. J. of Fracture Mechanics* **26**, 17–30.

Hertz, H. (1884) Über das gleichgewicht schwimmender elastischer Platten. *Weidemann's Annalen der Phys. und Chem.* **22**, 449.

Kerr, A. D. (1975) The bearing capacity of floating ice plates subjected to static and quasi-static loads: a critical survey. Research Report 333, U.S. Army Cold Regions Research and Engineering Laboratory, Hanover, New Hampshire.

Lichtenberger, G. J., Jones, J. W., Stegall, R. D. and Zadow, D. W. (1974) Static ice loading tests Resolute Bay—Winter 1973/74. APOA Project No. 64, Report No. 745B-74-14, Sunoco Science and Technology, Richardson, Texas (CRREL Bib #3095).

Meyerhof, G. G. (1960) Bearing capacity of floating ice sheets. *ASCE Journal of Engineering Mechanics* **86**(EM5), 113–145.

Michel, B. (1978) *Ice Mechanics*. Les Presses de l'Université Laval, Quebec, Canada.

Nevel, D. E. (1976) Creep theory of a floating ice sheet. Special Report 76–4, U.S. Army Cold Regions Research and Engineering Laboratory, Hanover, New Hampshire.

Peters, D. B., Ruser, J. R. and Watt, B. J. (1982) Rational basis for design of floating ice roads and platforms. *Proceedings, 14th Offshore Technology Conference*, pp. 153–167. Houston, Texas, OTC 4314, pp. 153–167.

Sinha, N. K. (1996) Elasto-delayed-elastic simulation of short-term deflection of fresh-water ice covers. *Cold Regions Science and Technology* **24**, 221–235.

Skrzypek, J. J. (1993) *Plasticity and Creep: Theory, Examples, and Problems* (English Edition) ed. R. B. Hetnarski. CRC Press, Boca Raton, Florida.

Slepyan, L. I. (1990) Modeling of fracture of sheet ice. *Izv. AN SSSR Mekhanika Tverdogo Tela* **25**(2), 151–157.

Sodhi, D. S. (1989) Interaction forces during vertical penetration of floating ice sheets with cylindrical indentors. *Proceedings, 8th International Conference on Offshore Mechanics and Arctic Engineering*, ed. N. K. Sinha, D. S. Sodhi and J. S. Chung, Vol. IV, pp. 377–382. The Hague, The Netherlands, American Society of Mechanical Engineers, New York.

Sodhi, D. S. (1995) Breakthrough loads of floating ice sheets. *ASCE Journal of Cold Regions Engineering* **9**(1), 4–22.

Sodhi, D. S. (1996) Deflection analysis of radially cracked floating ice sheets. *Proceedings, International Conference on Offshore Mechanics and Arctic Engineering*, ed. W. A. Nixon *et al.*, Florence, Italy, June 16–20, Vol. 4, pp. 97–101. American Society of Mechanical Engineers, New York.

Sodhi, D. S., Kato, K., Haynes, F. D. and Hirayama, K. (1982) Determining the characteristic length of model ice sheets. *Cold Regions Science and Technology* **6**, 99–104.

Timoshenko, S. and Woinowsky-Krieger, S. (1959) *Theory of Plates and Shells*, 2nd edn. McGraw-Hill Book Company, New York.

Westergaard, H. M. (1926) Stresses in concrete pavements computed by theoretical analysis. *Public Roads* **7**, 25–35.

Wyman, M. (1950) Deflections of an infinite plate. *Canadian Journal of Research* **A28**, 293–302.